

High-density accessible Ru-Se-Ni moieties Boosts the Hydrogen Evolution Reaction by Optimizing H Absorption

Shuang Ma,^{ab} Peiyong Yang,^{a,c} Jin Chang,^e Heng Zhang,^{d*} Mengjing Li,^a
Siqi Zhang,^a Jiafang Liu,^{f*} Fanghan Wang,^a Chuan Cheng,^a Ao Zhou,^a
Qingbin Li^{ab*}

^a. School of Chemical & Environmental Engineering (Key Lab of Ecological Restoration in Hilly Areas), Pingdingshan University, Pingdingshan, 467000, P.R. China, lqbsbc@126.com

^b. Yaoshan laboratory, Pingdingshan University, Pingdingshan Henan 467000, P.R. China,

^c. School of Innovation and Entrepreneurship, Pingdingshan University, Pingdingshan, 467000, P.R. China,

^d. College of Chemistry, Zhengzhou University, Zhengzhou 450001, P.R. China, hnzhangheng95@163.com

^e. School of Physics and Electronic Engineering, Xinyang Normal University, Xinyang 464000, P.R. China,

^f. Key Lab of Clean Energy and Green Circulation, College of Chemistry and Material Science, Huaibei Normal University, Anhui, Huaibei, 235000, P.R. China, ljf9791@126.com

1. Experiment

1.1. DFT calculations

DFT calculations in this work were carried out using the CASTEP program on Materials Studio.[1-2] The exchange-correlation effects were described by the Perdew-Burke-Ernzerhof functional within the generalized gradient approximation method.[3-4] The core-valence interactions were accounted by the projected augmented wave method.[5] The energy cutoff for plane wave expansions was set to 500 eV, and the $3\times 3\times 1$ Monkhorst-Pack grid k-points were selected to sample the Brillouin zone integration. The vacuum space is adopted 15 Å above the surface to avoid periodic interactions. The structural optimization was completed for energy and force convergence set at 1.0×10^{-5} eV and 0.02 eV Å⁻¹, respectively. The theoretical models were built based on the NiSe₂ (PDF #11-0552). The hydrogen absorption Gibbs free energy was calculated as the equation: $\Delta G_{H^*} = \Delta E - E(H_2)/2 + \Delta_{ZPE} - T\Delta S$, where the ΔE is the energy difference between the adsorption state and the pure surface. For the hydrogen adsorption ($(\Delta_{ZPE} - T\Delta S)$), the value of 0.24 eV was applied according to the report by Norskov et al. in 2005.[6]

1.2. Materials and Reagents

Nickel (II) nitrate hexahydrate [Ni(NO₃)₂·6H₂O], Ruthenium chloride hydrate (RuCl₃·3H₂O), selenium powder were obtained from Sinopharm Group Chemical Reagent. Potassium hydroxide (KOH), absolute ethanol and acetone were purchased from Beijing Chemical Works. Pt/C (20 wt. %) and Nafion (5 wt. %) were purchased from Sigma-Aldrich. All the reagents are analytical grade and used without further

treatment. Deionized water was employed as solvent.

1.3. Characterizations

The morphology and microstructure of all the samples were observed by scanning electron microscopy (SEM, Hitachi S4800) and transmission electron microscopy (TEM). The TEM samples were prepared by depositing a drop of the diluted suspension in ethanol on carbon film-coated copper grid. The high-resolution transmission electron microscopy (HRTEM, JEM-2010FEF) and were conducted on an FEI TECNAI F20 microscope at an acceleration voltage of 200 kV. Powder X-ray diffraction (XRD) patterns were collected on a Bruker D8 Advance. Field emission scanning electron microscopy (FESEM Zeiss Ultra Plus) was carried out to observe the surface morphology of samples. X-ray photoelectron spectroscopy (XPS) measurements were performed with a VG Scientific ESCALAB 210 electron spectrometer using Mg KR radiation under a vacuum of 2×10^{-8} Pa at 14 KV. Electron spin resonance was tested by a BRUCEREMXplus-9.5/12 spectrometer at 9.44 GHz and 300 K. The XAFS spectra at the Ru K-edge were recorded at the BL11B beamline of Shanghai Synchrotron Radiation Facility (SSRF). The incident photons were monochromatized by a Si(311) double-crystal monochromator. The energy calibration was performed using a Ru reference foil.

1.4. Electrochemical measurements

All the electrochemical measurements were performed on CHI 660E electrochemical workstation in a standard 3-electrode with 2-compartment cell. A Glassy carbon electrode with 3 mm diameter and a Hg/HgO electrode are used as

working electrode and the reference electrode, respectively. A graphite plate was used as the counter electrode in HER test. The as-prepared self-supporting catalysts were directly served as the working electrodes with a geometric area of 0.25 cm² and a catalyst loading of about 1.16 mg cm⁻². For comparison, a catalyst ink of commercial Pt/C (20 wt%) was prepared by ultra-sonic dispersion of 3 mg of catalyst in a solution of Nafion (20 μL)/water/isopropanol (980 μL, v/v ≈ 3:7). After obtaining a homogeneous dispersion, 100 μL of catalyst ink was loaded onto the NF. Linear sweep voltammeteries were performed at 5 mV/s in 1 M KOH.

In all measurements, the reference electrode was calibrated with respect to reversible hydrogen electrode (RHE). The HER potentials were converted to RHE scale according to the equation: $E \text{ (vs. RHE)} = E \text{ (vs. Hg/HgO)} + 0.059 \cdot \text{pH} + 0.098 \text{ V}$. The electrochemical double layer capacitance (C_{dl}) was determined with typical cyclic voltammetry measurements at various scan rates (10, 20, 30, 40 and 50 mV s⁻¹) in nonreactive region. The C_{dl} was further used to obtain the electrochemical active surface area (ECSA) values according to the equation: $\text{ECSA} = C_{dl}/C_s$, where C_s is the specific capacitance value of an ideal flat surface with a real surface area of 1 cm². In the estimate of ECSA, the general value of 40 μF cm⁻² was adopted for C_s . The Faradic efficiency is defined as the ratio of the amount of experimentally determined hydrogen to that of the theoretical value. The hydrogen gas was recorded synchronously. Then the moles of H₂ were calculated based on the gas laws. The theoretical amount of H₂ was then calculated by applying the Faraday law.

1.5 Mass activity

$$\text{Mass Activity (MA)} = \text{Catalytic Activity (CA)} / \text{Mass of Catalyst (MC)}$$

where catalytic activity is the rate of the target reaction (e.g., current density, reaction rate) obtained from the experimental data and mass of catalyst is the total mass of the Ru-NiSe₂/NF.

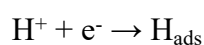
1.6 Kinetic analysis

The Tafel equation is generally applied to evaluate the kinetic properties of HER process, which could be expressed as below:

$$\eta = a + b \times \log(j)$$

where η , j , a and b are the overpotential, current density, constants and the Tafel slope, respectively. The Tafel slope is directly associated with the specific reaction pathways and can give insights into the rate-determining step of HER process. Generally, there are three typical primary steps for the HER process:

Volmer reaction: Proton is reduced to form adsorbed hydrogen (H_{ads}):



Heyrovsky reaction: Another proton reacts with the H_{ads} to form hydrogen gas:



Tafel reaction: Two H_{ads} combine to form hydrogen gas:



Based on the value of the Tafel slope, the rate-determining step could be determined as follows[7]:

- (1) If $b \approx 120$ mV/dec, the Volmer step is rate-determining.
- (2) If $b \approx 40$ mV/dec, the Heyrovsky step is rate-determining.
- (3) If $b \approx 30$ mV/dec, the Tafel reaction is rate-determining.

2. Figures and tables

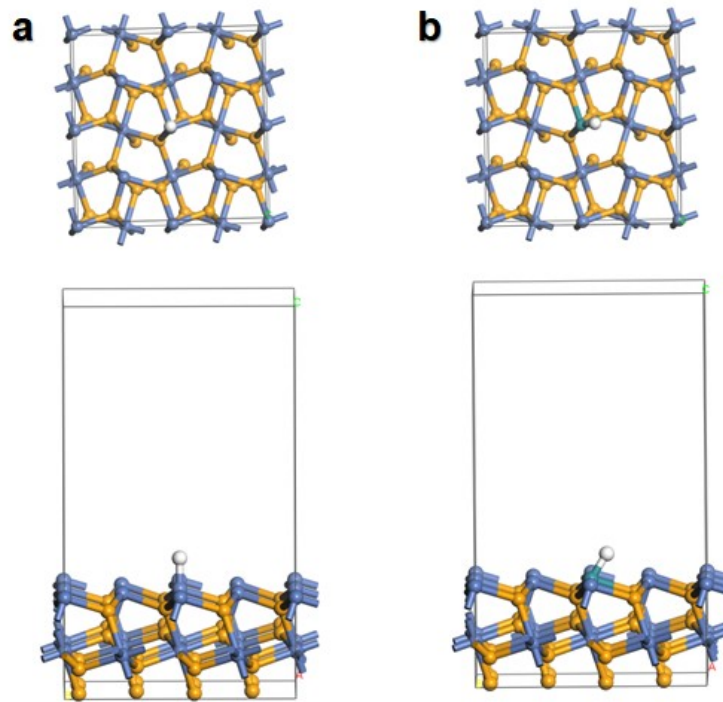


Fig. S1. The model of H adsorption on Ru-NiSe₂/NF and NiSe₂/NF surface.

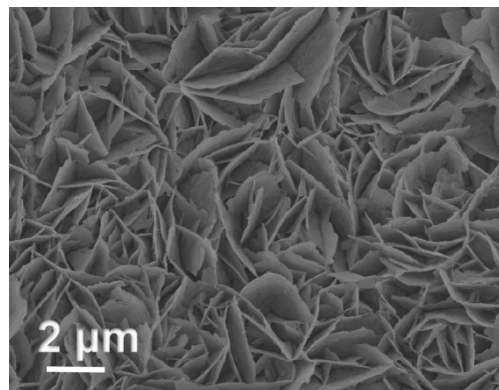


Fig. S2. SEM image of NiSe₂/NF.

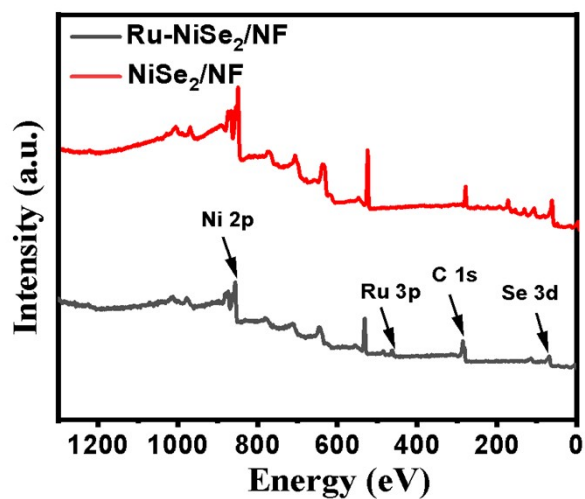


Fig. S3. XPS survey of Ru-NiSe₂/NF and NiSe₂/NF.

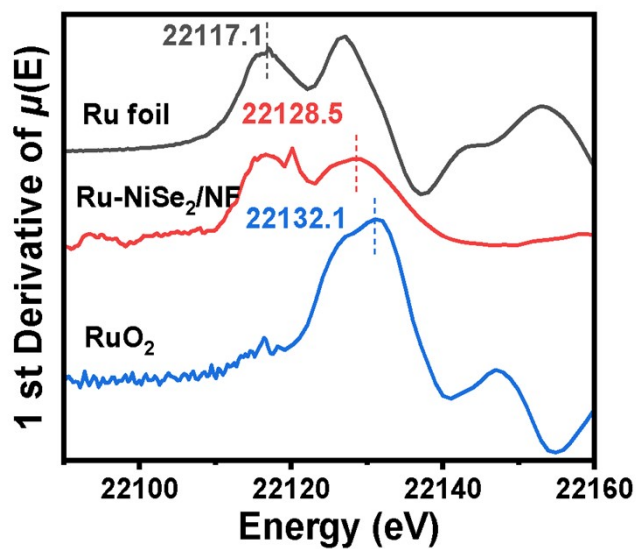


Fig. S4. First derivatives from the Ru K-edge XANES spectra of Ru-NiSe₂/NF, RuO₂, and Ru foil.

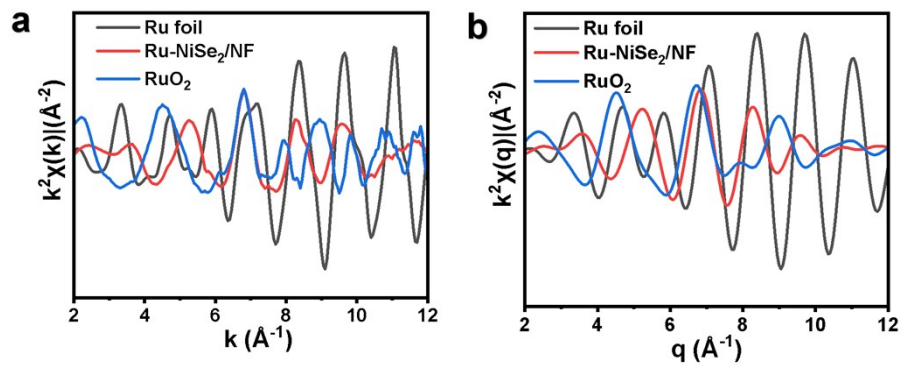


Fig. S5. EXAFS curves at the k space and q space of Ru-NiSe₂/NF RuO₂ and Ru foil.

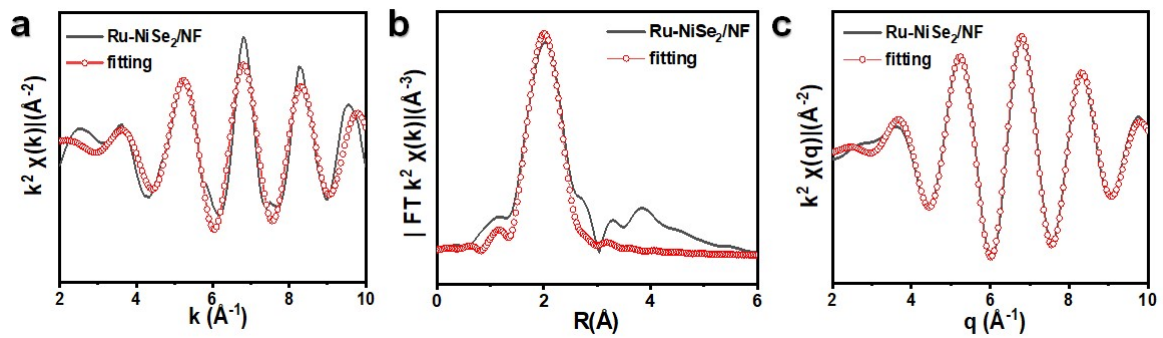


Fig. S6. EXAFS fitting curves of Ru-NiSe₂/NF at a) k space b) R space and c) q space.

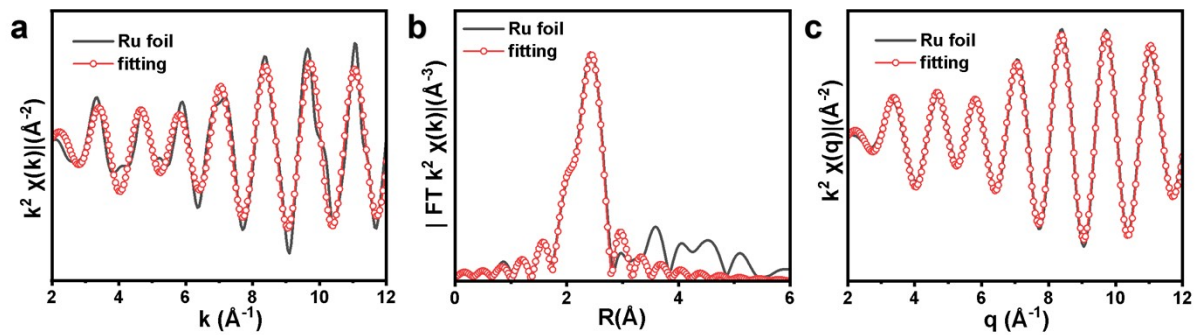


Fig. S7. EXAFS fitting curves of Ru foil at a) k space b) R space and c) q space.

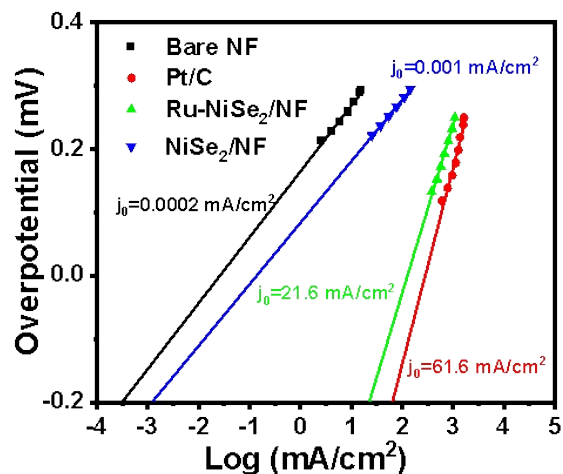


Fig. S8. the exchange current density of Ru-NiSe₂/NF, NiSe₂/NF, Pt/C and Bare NF.

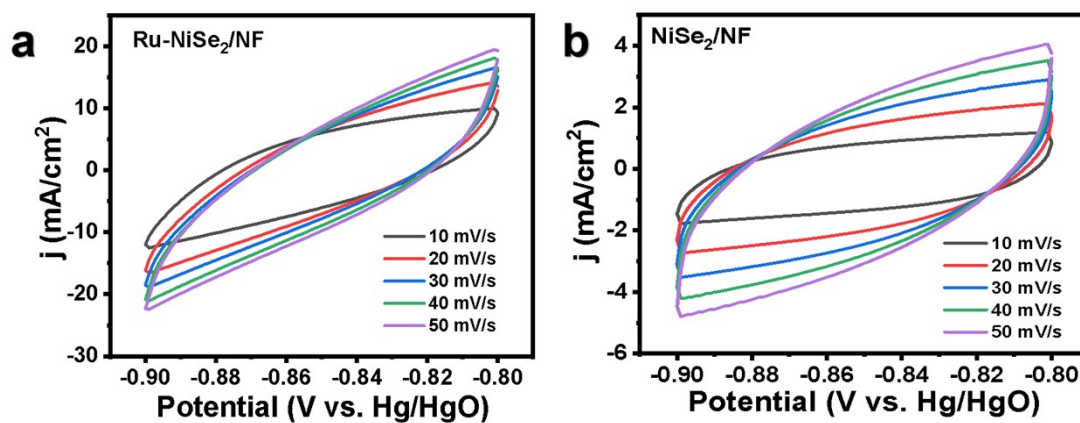


Fig. S9. Cyclic voltammogram (CV) curves of a) Ru-NiSe₂/NF and b) NiSe₂/NF at different scan rates in alkaline media.

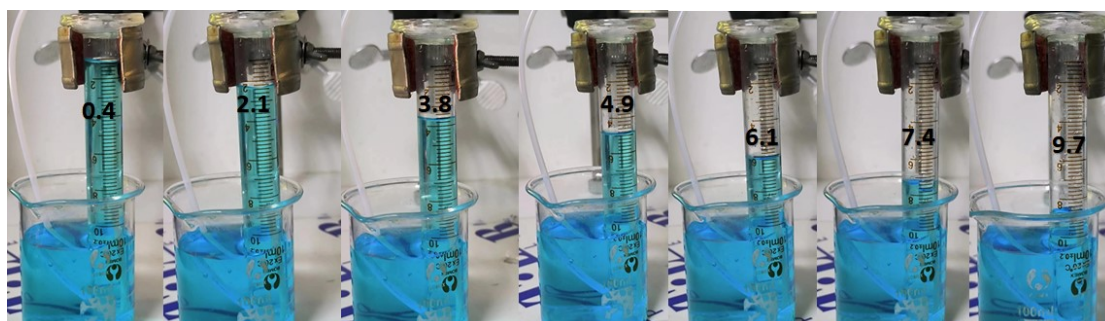


Fig. S10. Amount of H₂ generation experimentally for Ru-NiSe₂/NF in 1M KOH.

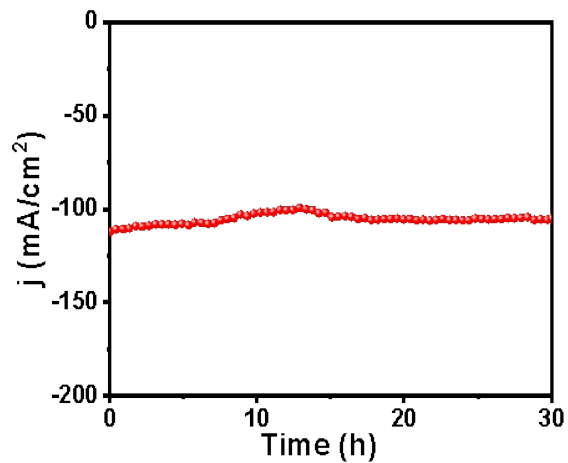


Fig. S11. Chronopotentiometry curves of Ru-NiSe₂/NF at -0.1 V vs RHE.

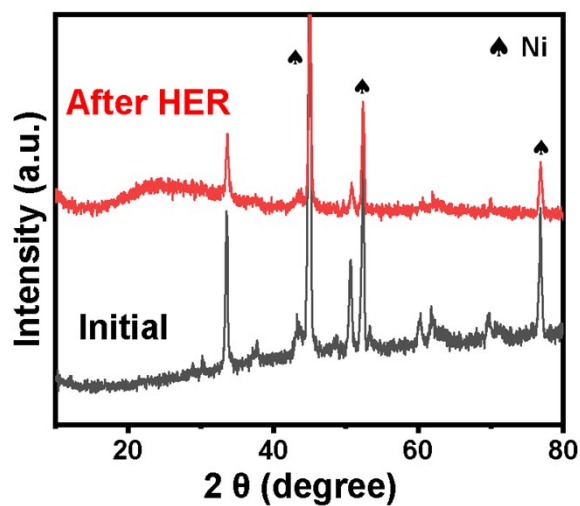


Fig. S12. The XRD pattern of the Ru-NiSe₂/NF after long time durability test in 1 M KOH.

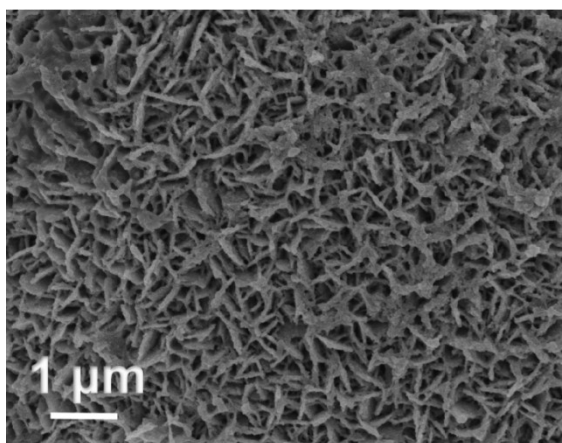


Fig. S13. SEM image of Ru-NiSe₂/NF after test for 60 h.

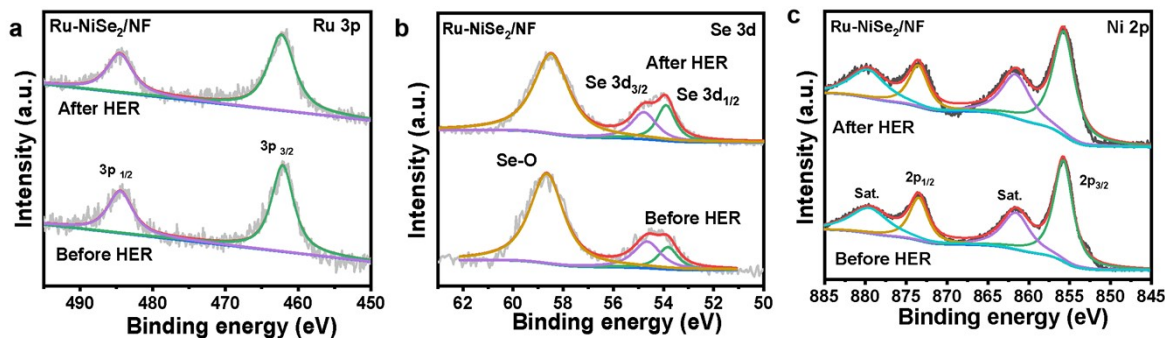


Fig. S14. The XPS spectra of Ru-NiSe₂/NF before and after long-term test.

Table 1. Structural parameters of different samples extracted from the EXAFS fitting.

Sample	shell	CN	R(Å)	σ^2 (10^{-3}Å^2)	ΔE_0 (eV)	R factor
Ru foil	Ru-Ru	12.0	2.67	3.1	4.2	0.016
Ru-NiSe ₂ /NF	Ru-Se	4.25	2.54	12.6	-5.6	0.011

S_0^2 is the amplitude reduction factor; CN is the coordination number; R is interatomic distance (the bond length between central atoms and surrounding coordination atoms); σ^2 is Debye-Waller factor (a measure of thermal and static disorder in absorber-scatterer distances); ΔE_0 is edge-energy shift (the difference between the zero kinetic energy value of the sample and that of the theoretical model). R factor is used to value the goodness of the fitting.

* This value was fixed during EXAFS fitting, based on the known structure.

Error bounds that characterize the structural parameters obtained by EXAFS spectroscopy were estimated as $N \pm 20\%$; $R \pm 1\%$; $\sigma^2 \pm 25\%$; $\Delta E_0 \pm 10\%$.

Ru-NiSe₂ (FT range: 2.4-9.5 Å⁻¹; fitting range: 1.2-2.5 Å)

Ru foil (FT range: 3.0-12.0 Å⁻¹; fitting range: 1.0-3.0 Å)

Table S2. HER comparison in 1.0 KOH with the recently reported literatures.

Materials	Tafel slope (mV dec ⁻¹)	η_{10} / mV	Reference
Ru-NiSe₂/NF	39.3	36	This work
Ru-Ni ₃ N	55	51	[8]
RuP/NPC	123	168	[9]
Ru SAs-Ni ₂ P	75	57	[10]
Sr ₂ RuO ₄	61	51	[11]
Cu _{2-x} S@Ru NPs	48	82	[12]
RuO ₂ -NWs@g-CN	70	95	[13]
Ru/Co ₄ N-CoF ₂	144	53	[14]
Ru-NPs/SAs@N-TC	58	97	[15]
CF@Ru-CoCH	65	66	[16]
Ru/Mo ₂ CT _x	57	73	[17]
Ru/NSC-200	42	50	[18]
Ru SAs/N-Mo ₂ C NSs	38	53	[19]
Ni ₅ P ₄ -Ru/CC	52	54	[20]
Ru ₂ Ni ₂ SNs	23.4	40	[21]
S-RuP@NPSC	90	92	[22]
RuP _x NPs	70	74	[23]
Ru-MoS ₂ /CNT	62	50	[24]

Reference:

1. G. Kresse, J. Hafner, Ab Initio Molecular Dynamics for Liquid Metals, *Phys. Rev. B*, 1993, **47**, 558-561.
2. G. Kresse, J. Hafner, Ab Initio Molecular-Dynamics Simulation of the Liquid-Metal Amorphous-Semiconductor Transition in Germanium, *Phys. Rev. B*, 49 1994, **49**, 14251-14269.
3. J. P. Perdew, K. Burke, M. Ernzerhof, Generalized Gradient Approximation Made Simple, *Phys. Rev. Lett.*, 1996, **77**, 3865-3868.

4. G. Kresse, D. Joubert, From Ultrasoft Pseudopotentials to the Projector Augmented Wave Method., *Phys. Rev. B*, 1999, **59**, 1758-1775.
5. P. E. Blöchl, Projector Augmented-Wave Method, *Phys. Rev. B*, 1994, **50**, 17953-17979.
6. J. K. Nørskov, T. Bligaard, A. Logadottir, J. R. Kitchin, J. G. Chen, S. Pandalov, U. Stimming, Trends in the Exchange Current for Hydrogen Evolution. *J. Electrochem. Soc.*, 2005, **152**, J23-J26.
7. N. Mahmood, Y. Yao, J.-W. Zhang, L. Pan, X.W. Zhang, J.-J. Zou, Electrocatalysts for hydrogen evolution in alkaline electrolytes: mechanisms, challenges, and prospective solutions, *Adv. Sci.*, 2018, **5**, 1700464.
8. X. Gao, W. Zang, X. Li, Z. Wang, L.R. Zheng, Z. Kou, Achieving efficient alkaline hydrogen evolution reaction on long-range Ni sites in Ru clusters-immobilized Ni₃N array catalyst. *Chem. Eng. J.*, 2023, **451**, 138698.
9. Q. Qin, H. Jang, L. Chen, G. Nam, X. Liu, J. Cho, Low Loading of RhxP and RuP on N, P Codoped Carbon as Two Trifunctional Electrocatalysts for the Oxygen and Hydrogen Electrode Reactions, *Adv. Energy Mater.*, 8 (2018) 1801478.
10. K. Wu, K. Sun, S. Liu, W.-C. Cheong, Z. Chen, C. Zhang, Y. Pan, Y. Cheng, Z. Zhuang, X. Wei, Y. Wang, L. Zheng, Q. Zhang, D. Wang, Q. Peng, C. Chen and Y. Li, *Nano energy*, 2021, **80**, 105467.
11. Y. Zhu, H. A. Tahini, Z. Hu, J. Dai, Y. Chen, H. Sun, W. Zhou, M. Liu, S. C. Smith, H. Wang and Z. Shao, Unusual synergistic effect in layered Ruddlesden–Popper oxide enables ultrafast hydrogen evolution, *Nat. Commun.*, 2019, **10**, 149.
12. D. Yoon, J. Lee, B. Seo, B. Kim, H. Baik, S. H. Joo and K. Lee, Cactus-Like Hollow Cu_{2-x}S@Ru Nanoplates as Excellent and Robust Electrocatalysts for the Alkaline Hydrogen Evolution Reaction, *Small*, 2017, **13**, 1700052.
13. T. Bhowmik, M. K. Kundu and S. Barman, Growth of One-Dimensional RuO₂ Nanowires on gCarbon Nitride: An Active and Stable Bifunctional Electrocatalyst for Hydrogen and Oxygen Evolution Reactions at All pH Values, *ACS Appl. Mater. Interfaces*, 2016, **8**, 28678.

14. S. Zhou, H. Jang, Q. Qin, Z. Li, M.G. Kim, X. Ji, X. Liu and J. Cho, Ru atom-modified Co₄N-CoF₂ heterojunction catalyst for high-performance alkaline hydrogen evolution, *Chem. Eng. J.*, 2021, **414**, 128865.
15. B. Yan, D. Liu, X. Feng, M. Shao, and Y. Zhang, Ru Species Supported on MOF-Derived N-Doped TiO₂/C Hybrids as Efficient Electrocatalytic/Photocatalytic Hydrogen Evolution Reaction Catalysts *Adv. Funct. Mater.* 2020, **30**, 2003007.
16. J. Li, Q. Zhou, Z. Shen, S. Li, J. Pu, C. Zhong, M. Cao, X. Jing, H.G. Zhang, Y.Y. Wang, H.X. Ma, Synergistic effect of ultrafine nano-Ru decorated cobalt carbonate hydroxides nanowires for accelerated alkaline hydrogen evolution reaction, *Electrochim. Acta.*, 2020, **331**, 135367.
17. Y. Wu, L. Wang, T. Bo, Z. Chai, J.K. Gibson, W. Shi, Boosting Hydrogen Evolution in Neutral Medium by Accelerating Water Dissociation with Ru Clusters Loaded on Mo₂CT_x MXene, *Adv. Funct. Mater.*, 2023, **33**, 2214375.
18. M. Khalid, H.A.B. Fonseca, L.G. Verga, M.R. Hatshan, J.L.F. Silva, H. Varela, S. Shahgaldi, Facile synthesis of Ru nanoclusters embedded in carbonaceous shells for hydrogen evolution reaction in alkaline and acidic media, *Electroanal. Chem.* 2023, **929**, 117116.
19. J. Yu, A. Wang, W. Yu, X. Liu, X. Li, H. Liu, Y. Hu, Y. Wu and W. Zhou, Tailoring the ruthenium reactive sites on N doped molybdenum carbide nanosheets via the anti-Ostwald ripening as efficient electrocatalyst for hydrogen evolution reaction in alkaline media, *Appl. Catal. B-Environ.*, 2020, **277**, 119236.
20. Q. He, D. Tian, H. Jiang, D. Cao, S. Wei, D. Liu, P. Song, Y. Lin, L. Song, Achieving Efficient Alkaline Hydrogen Evolution Reaction over a Ni₅P₄ Catalyst Incorporating Single-Atomic Ru Sites, *Adv. Mater.*, 2020, **32**, 1906972.
21. J. Ding, Q. Shao, Y. Feng and X. Huang, Ruthenium-nickel sandwiched nanoplates for efficient water splitting electrocatalysis, *Nano Energy* 2018, **47**, 1-7.
22. X. Liu, F. Liu, J. Yu, G. Xiong, L. Zhao, Y. Sang, S. Zuo, J. Zhang, H. Liu, W. Zhou, Charge Redistribution Caused by S, P Synergistically Active Ru Endows an Ultrahigh Hydrogen Evolution Activity of S-Doped RuP Embedded in N,P,S-Doped Carbon, *Adv. Sci.*, 2020, **7**, 2001526.

23. J.-Q. Chi, W.-K. Gao, J.-H. Lin, B. Dong, K.-L. Yan, J.-F. Qin, B. Liu, Y.-M. Chai and C.-G. Liu, Hydrogen Evolution Activity of Ruthenium Phosphides Encapsulated in Nitrogen- and Phosphorous-Codoped Hollow Carbon Nanospheres, *ChemSusChem* 2018, **11**, 743-752.
24. X. Zhang, F. Zhou, S. Zhang, Y. Liang and R. Wang, Engineering MoS₂ Basal Planes for Hydrogen Evolution via Synergistic Ruthenium Doping and Nanocarbon Hybridization, *Adv. Sci.*, 2019, **6**, 1900090.